*International Journal of Heat and Fluid Flow (2013) xxx-xxx; DOI: http://dx.doi.org/10.1016/j.ijheatfluidflow.2013.10.005*

# IR Measurements of the Thermodynamic Effects in Cavitating flow

**MARTIN PETKOVŠEK[1] & MATEVŽ DULAR[1]**

[1] Laboratory for Water and Turbine Machines, University of Ljubljana, Askerceva 6, 1000 Ljubljana, SI-Slovenia

(Received 23 April 2013; revised 13 September 2013; accepted 14 October 2013)

The understanding of the thermodynamic effects of cavitating flow is crucial for applications like turbopumps for liquid hydrogen LH2 and oxygen LOx in space launcher engines. Experimental studies of this phenomenon are rare as most of them were performed in the 1960's and 70's. The present study presents time resolved IR (Infra-Red) measurements of thermodynamic effects of cavitating flow in a Venturi nozzle.

Developed cavitating flow of hot water (95°C) was observed at different operating conditions – both conventional high speed visualization and high speed IR thermography were used to evaluate the flow parameters.

Both the mean features of the temperature distributions and the dynamics of the temperature field were investigated. As a result of evaporation and consequent latent heat flow in the vicinity of the throat a temperature depression of approximately 0.4 K was measured. In the region of pressure recuperation, where the cavitation structures collapse, the temperature rise of up to 1.4 K was recorded. It was found that the temperature dynamics closely follows the dynamics of cavitation structures.

Finally experimental results were compared against a simple model based on the Rayleigh-Plesset equation and the thermal delay theory and plausible agreement was achieved.

Experimental data is most valuable for further development of numerical models which are, due to poor ensemble of existing experimental results, still at a very rudimentary level.

**Key words:** Cavitation, Thermodynamic effects, hot water, thermal delay, Venturi channel



## 1 Introduction

Cavitation is characterized by vapor generation and condensation due to pressure changes at approximately constant temperature of the fluid. Is it justified to use the isothermal approach when we are dealing with liquids such as cold water, where the influence of the temperature variations on the integral liquid properties is

negligible (Hord *et al.* 1972).

A detailed look in the formation of a cavitation bubble shows that it is formed by the local pressure drop, which causes the gas inside the cavitation nucleus to expand what consequently triggers evaporation. The latent heat is then supplied from the surrounding liquid, creating a thermal boundary layer around the bubble. The heat transfer causes a local decrease of the liquid temperature, which results in a slight drop of the vapour pressure (Franc & Michel 2004). This phenomenon delays the further development of the bubble, because now a greater pressure drop is needed to maintain the process. This phenomenon is known as thermal delay (Brennen 1995).

When the local surrounding pressure rises, the bubble starts to collapse. During the collapse the condensation occurs and in the final stages the gases also violently compress, which leads to considerable rise of the temperature inside the bubble (Hauke *et al.* 2007).

As a rule of a thumb the thermodynamic effects can usually be neglected in fluids for which the critical point temperature is much higher than the working temperature. However, the effects become significant when the critical point temperature is close to the temperature of the fluid, like in case of cryogenic fluids (Stahl & Stepanoff 1956). By formation of cavitation bubble in cryogenic liquids a significant temperature drop occurs, which causes a delay in development of the bubble. The understanding of this thermodynamic effect is therefore crucial for example in turbopumps for liquid hydrogen LH2 and oxygen LOx in space launcher engines – particularity well known is the failure of the Japanese H-II rocket due to rotating cavitation in the LH2 turbopump (Sekita *et al.* 2001). Consequently, nowadays much effort is put into development of CFD (Computational Fluid Dynamics) methods for the prediction of thermodynamic effects of cavitation of cryogenic fluids (Utturkar *et al.* 2005, Hosangadi & Ahuja 2005, Goncalvès & Fortes Patella 2010, 2011, Goncalvès *et al.* 2010).

The first study, where the thermodynamic effects on pump performance were considered, was conducted by Stahl & Stepanoff (1956). Sarodsy & Acosta (1961) reported significant difference in the appearance of cavitation in water and in refrigerant Freon. The thermodynamic effects were experimentally quantified by Ruggeri & Moore (1969) who investigated the variations of pump performance for various temperatures, fluids and operating conditions. The most extensive experiments on cryogenic cavitation were conducted by Hord *et al.* (1972, 1973a, 1973b). His results, acquired in Venturi nozzle, and on hydrofoil and ogive models are still considered as a benchmark for validating numerical models for thermodynamic effects in cavitation. Recent investigations have focused on the influence of the thermodynamic effects on performance and cavitation instabilities in rotating machinery. Franc *et al.* (2004) analyzed the cavitation instabilities on an inducer in water and in refrigerant R114. A similar study was conducted by Cervone *et al.* (2005) with cold and hot water at 293 K and 343 K, respectively.

Due to complexity of the experimental investigation of the local temperature variations, the past studies mostly concentrated on the consequences of the thermodynamic effects, rather than on the investigation of the mechanism itself. Fruman *et al.* (1999) measured the local wall temperature under the cavity with five micro-thermocouples. More recently, measurements of the temperature depression within the sheet cavity at the leading edge of inducer blades were conducted by Franc *et al.* (2010). Rimbert et al. (2012) locally measured the temperature by two-color laser in a micro cavitation channel, and investigated the relationship between the void fraction and the temperature variation. Meanwhile Dular & Coutier-Delgosha (2012) used a high-speed infrared (IR) camera to measure the temperature on a single cavitation bubble.

Until now the thermodynamic effects were usually estimated by rudimentary models, which most of them were proposed between 1960 and 1990. The most commonly used parameter is the B-factor, which is a dimensionless temperature depression proposed by Stepanoff (1961). Brennen (1973) defined the $\Sigma$ parameter, which depends only on fluid temperature, a similar parameter $\alpha$ was proposed by Kato (1984) and Watanabe et al. (2007) proposed a non-dimensional $\Sigma^*$ parameter.

The present study shows innovative, direct measurement of thermodynamic effects in cavitating flow by a non-invasive method. A high speed IR camera was used to measure the temperature field in the cavitating flow; simultaneously visualization by a conventional high-speed camera was made.

## 2 Measurements

Experiments were conducted at the University of Ljubljana in Laboratory for Water and Turbine Machines.

### 2.1 Experimental set-up and the Venturi geometry

The experimental set-up is shown in Fig. 1.

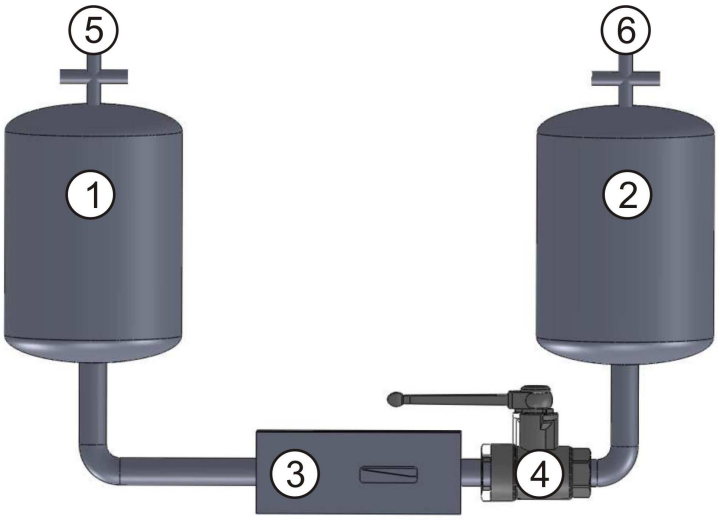


**Figure 1:** Experimental set-up.

The cavitation tunnel consists of two 2 L reservoirs (1 and 2), a convergent-divergent Venturi nozzle (3) and a ball valve (4). The first reservoir (1) is filled with the working fluid (hot water) and pressurized to the desired level (through pressure pipe connection (5)). Similarly, in the second, empty, reservoir (2), the pressure level can also be adjusted by the second pressure pipe (6). At a rapid opening of the ball valve (4), the working fluid is pushed from the first reservoir through the Venturi nozzle (3), where the cavitation occurs, to the second reservoir (2). During the 3 to 5 second long experiment the pressures in both reservoirs were recorded by Hygrosens DRTR-AL-10V-R16B pressure transmitters at a rate of 1000 Hz.

The geometry of the Venturi test section is shown in Fig. 2. The constriction with a converging angle of 18° and diverging angle of 8° was used. The channel of the test section was machined (milled) out of three aluminum blocks and later polished by 1μm emulsion. The section itself is made from two parts – lower, with the converging/diverging walls and upper, straight part. This enabled machining of a sharp transition between the converging and diverging part of the Venturi (the radius at the throat was made as small as possible – about 0.2 mm). The cross-section of the test section channel is reduced from $6\times5mm^2$ at the inlet, to the $1\times5mm^2$ at the throat.

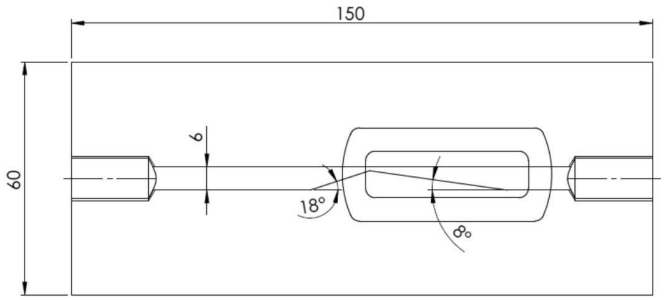


**Figure 2:** Convergent-divergent Venturi nozzle (the flow direction is from the left to the right).

Downstream of the throat of the Venturi nozzle an observation window, made out of sapphire glass, was installed – sapphire glass had to be used since it is transparent in both visible and infrared light spectrum.

The flow velocity changes during the experiment as a result of changing pressure difference between the two reservoirs. Nevertheless, during a short period of time (about 0.3s) the pressure difference remained constant at a desired level so that measurement point could be easily determined.
Developed cavitating flow was observed at several pressure differences which give values of cavitation number (1.3, 1.8 and 2.3). These were defined as the difference between the pressure in the first reservoir $p_1$ and vapour pressure $p_v$ ($p_v$(95°C) =84513 Pa) divided by the difference in pressure between the two reservoirs ($p_1$-$p_2$):

$$\sigma = \frac{p_1 - p_v}{p_1 - p_2} \qquad (1)$$

Decreasing the cavitation number, results in higher probability in cavitation occurrence or in an increase of the magnitude of the already present cavitation. Considering the combination of inaccuracies of pressure and temperature measurements, the cavitation number could be determined within ±0.02 of global uncertainty.

The parameters of the experiments can be found in Table 1.

**Table 1:** Parameters of investigated cavitation conditions.

| Test | $p_1$ (Pa) | $p_2$ (Pa) | σ (-) |
|---|---|---|---|
| 1 | 740000 | 233000 | 1.3 |
| 2 | 695500 | 356000 | 1.8 |
| 3 | 690000 | 427000 | 2.3 |

Figure 3 shows about one period of cavitation cloud shedding process at cavitation number $\sigma$ = 1.3.

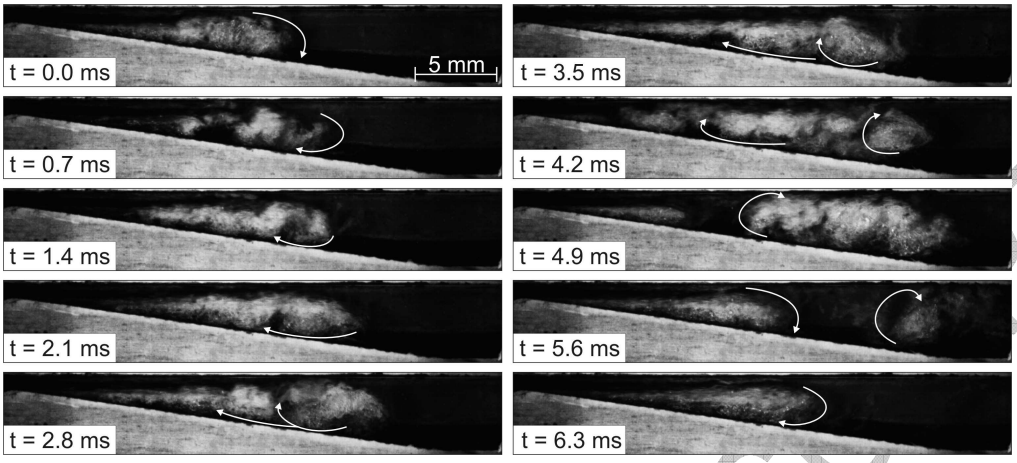


**Figure 3:** Cavitation as seen at cavitation number $\sigma$ = 1.3 (the flow direction is from the left to the right).

One can see that cavitation is first attached (at t = 0.0 ms). It then slowly grows while at its closure a reentrant jet forms – it flows upstream and consequently causes the cavitation cloud to separate (at this instant at t = 4.2 ms the maximum size of the attached part of the cavity is reached). The cloud separates from the attached cavity at t = 4.9 ms. Interestingly, it seems that at t = 2.8 ms the reentrant jet splits into two branches – a more persistent branch travels further upstream and causes the large cloud separation, wile the smaller one dies out at t = 4.9 ms. Branching of the reentrant jet may be due to its confinement in a very small test section (Dular *et al.* 2010). While the separated cloud flows downstream and collapses in the higher pressure region the attached cavity begins to grow again and the process is repeated. With the cavitation cloud shedding frequency (from Fig. 7 we get f=166 Hz), its maximal attached length (l=0.035 m) and flow velocity of the jet (v =17 m/s) one can than calculate the Strouhal number ($St = (f \cdot l)/v$) to be approximately St=0.34, which points to a fully developed cavitating flow regime (St values between 0.2 and 0.6 are associated with fully developed cavitating flow regime (Dular & Bachert 2009)).

**2.2 Cavitation visualization and temperature measurements**

Fastec Imaging HiSpec4 2G mono high speed camera was used to capture images of cavitating flow from the side view. The camera enables capturing images at 523 fps (frames per second) at 3Mpixel resolution. For the present experiments, it was synchronized with the IR camera and recorded at a higher frame rate (up to 10000 fps) and reduced resolution with exposure time of 10 μs.

A high-speed IR camera CMT384SM – Thermosensorik was used to record the dynamics of the temperature fields. The camera is sensitive in wavelength range between 3 and 5 μm.

Even a very thin layer of water (10 μm or even less) is absolutely opaque in the infra red wavelength range (Hale & Querry 1973). Hence the method enables temperature measurements only within the
layer close to the sapphire glass and water or, in the event when a bubble is in a direct contact with the glass, on the bubble interface with the water (water vapour is transparent in the wavelength from 3 and 5 μm). Results of a study by Dular & Coutier-Delgosha (2012), where single cavitation bubbles were observed, showed that the recorded temperatures at the bubble interface and in the liquid boundary layer do not significantly differ. Also, due to the small size of the section, highly turbulent flow and extensive cavitation zone, which engulfs a large part of the section, one can expect a homogeneous temperature profile over the width of the Venturi (the thickness of the thermal boundary was estimated to $\delta = 3$ μm).

Two different acquisition frequencies of the IR camera were applied during the experiments. At a low frequency of 790 fps, the average features of temperature field were obtained at a relatively high spatial resolution. The frame size at this frequency was 288×64 pixels (the acquisition window extended over the whole observable part of the Venturi section).
To analyze the dynamics of the temperature field and its relationship to the cavitation structure dynamics a higher frequency (3550 fps) of the acquisition was chosen. Consequently the frame size (acquisition window) had to be reduced down to 96×16 pixels.
The pixel size and the integration time were the same for both settings – one pixel corresponded to about 0.16×0.16 $mm^2$ area and the integration time was 50 μs.

The uncertainty of IR temperature measuring was inspected by comparison with measurements by an A-class Pt100 sensor and a discrepancy of ±0.2 K was found. However, our main goal was to quantify relative differences in non-uniform (and possibly time-dependant) temperature field. For a single element on the temperature sensor of the IR camera, the noise equivalent temperature difference (NETD) was less than 20 mK.

**3 Theoretical background**

Theoretical approach of the process of bubble expansion and implosion, which is investigated here, can be found for example in Brennen (1995) or Franc & Michel (2004). When the pressure drops, the bubble begins to grow due to both water evaporation and gas expansion (expansion of the air contained inside the initial nucleus). During the collapse, the process is reversed – the main mechanisms are now condensation of vapor and compression of gases. In both phenomena, the magnitude of temperature variations in the thermal layer around the bubble depends strongly on the predominant process that drives the bubble size evolution: gas expansion/compression and the phase changes. One can estimate the characteristic time of the heat transfer process at the bubble interface $\Delta t_r$ (Franc & Michel 2004):

$$\Delta t_r = \frac{\left(\rho_g c_{vg} R\right)^2}{9\lambda_l \rho_l c_{pl}}, \tag{2}$$

where $\rho_g$ and $\rho_l$ are the gas (vapour) and liquid densities, $c_{vg}$ and $c_{pl}$ are the gas (vapour) and liquid heat capacities, R is the maximum bubble radius and $\lambda_l$ is the heat conductivity of the liquid. The process can be considered adiabatic if the bubble life time is much shorter that the characteristic time of heat transfer $\Delta t_r$ - the bubble evolution is then mainly driven by expansion and compression of gases. In the opposite case, if there is enough time for the heat transfer to proceed until thermal equilibrium is reached, the process is closer to isothermal conditions, which means that evaporation and condensation of water and water vapour are the main driving mechanisms.

In the present experiments, a typical bubble in water at 95°C grew and collapsed in about 0.2 ms and its maximum diameter was in the order of 10 μm. Considering Eqn. 2 with $\rho_l$ = 961.9 kg/m$^3$, $\rho_v$ = 0.4957 kg/m$^3$, $c_{pl}$ = 4211 J/kg/K, $c_{vg}$ = 720 J/kg/K and $\lambda_l$ = 0.5275 W/m/K, $\Delta t_r \approx$ 0.66 ps is obtained. This is obviously much smaller than the time of bubble life (0.2 ms), which means that that evaporation and condensation can be considered the driving processes involved in the evolution of the bubbles in the present study. As a conclusion one can claim that the thermal delay theory, which is described in the following section, can be applied to interpret the results of the measurements.

### 3.1 Theory of thermal delay

The idea of thermal delay can be most simply presented in the case of a spherical bubble in an infinite liquid. As the pressure at the infinity drops, an initial spherical nucleus begins to grow. The evaporation process involved in this growth requires the latent heat *L* to be supplied by the liquid at the bubble interface which gives estimation for the temperature difference (Brennen 1995):

$$\Delta T = T_b - T_\infty = -\frac{\dot{R}\sqrt{t}}{\sqrt{\alpha_l}} \frac{\rho_v L}{\rho_l c_{pl}}, \tag{3}$$

where the thermal diffusivity of the liquid $\alpha_l$ is defined as $\alpha_l = \frac{\lambda_l}{\rho_l c_{pl}}$. Brennen (1995) introduced the parameter $\Sigma$ which is given by:

$$\Sigma = \frac{(\rho_v L)^2}{\rho_l^2 c_{pl} T_\infty \sqrt{\alpha_l}}. \quad (4)$$

If one assumes the bubble to remain spherical the Rayleigh-Plesset equation (Plesset 1949) including thermal effects can be derived (Brennen 1995):

$$\rho_l\left(R\ddot{R} + \frac{3}{2}\dot{R}^2\right) + \Sigma\dot{R}\sqrt{t}\rho_l = p_v(T_\infty) - p_\infty + p_{g0}\left(\frac{R_0}{R}\right)^{3\gamma} - \frac{2S}{R} - 4\mu\frac{\dot{R}}{R}, \quad (5)$$

which gives the bubble radius evolution according to time t ($p_{g0}$ is the initial gas pressure in the bubble, S is the surface tension, and μ is the viscosity of the liquid).

In Section 5, Eqn. 5 is solved numerically to obtain the bubble radius evolution as a function of time. Then Eqn. 3 is applied to calculate the time evolution of the temperature $\Delta T$. Results are finally compared against the measurements.

**4 Experimental results**

As already mentioned two sets of measurements were conducted. We first investigated the mean features of the temperature fields at a low acquisition frequency, later we increased the frame rate of the IR camera to capture the temperature dynamics of cavitating flow.

**4.1 Mean temperature fields**

The experiment was designed to operate over a short duration after which the reservoirs needed to be repressurized; based on observation of the pressure evolution in both tanks we concluded that during a short period of time (0.3 s) constant flow conditions were achieved. Since cavitation exhibited the shedding frequency of 166 Hz and more, this was enough to acquire representative ensemble of results.

During this set of experiments conventional and IR high speed cameras operated at 10000 and 790 fps, respectively. Figure 4 shows a representative instantaneous image of cavitation (a), a mean of a series of cavitation images (b) and the mean temperature field in the layer near the sapphire window (c) for cavitation numbers σ = 1.3 (top), 1.8 (middle) and 2.3 (bottom). The flow is from the left to the right; x = 0 mm corresponds to the position of the throat of the Venturi channel. The reference temperature $T_\infty$ of approximately 95°C (slight variations (±1 K), which do not influence the magnitude of the thermodynamic effects, appeared between the tests) was measured 20 mm upstream of the throat of the Venturi by a type J thermocouple. This temperature was subtracted from the measured temperature to obtain data in terms of the temperature change ΔT.

In the temperature diagram at σ = 1.3 a line through the mid height of the channel is plotted – the temperature evolutions shown in Figs. 5, 7 and 8 correspond to this line.

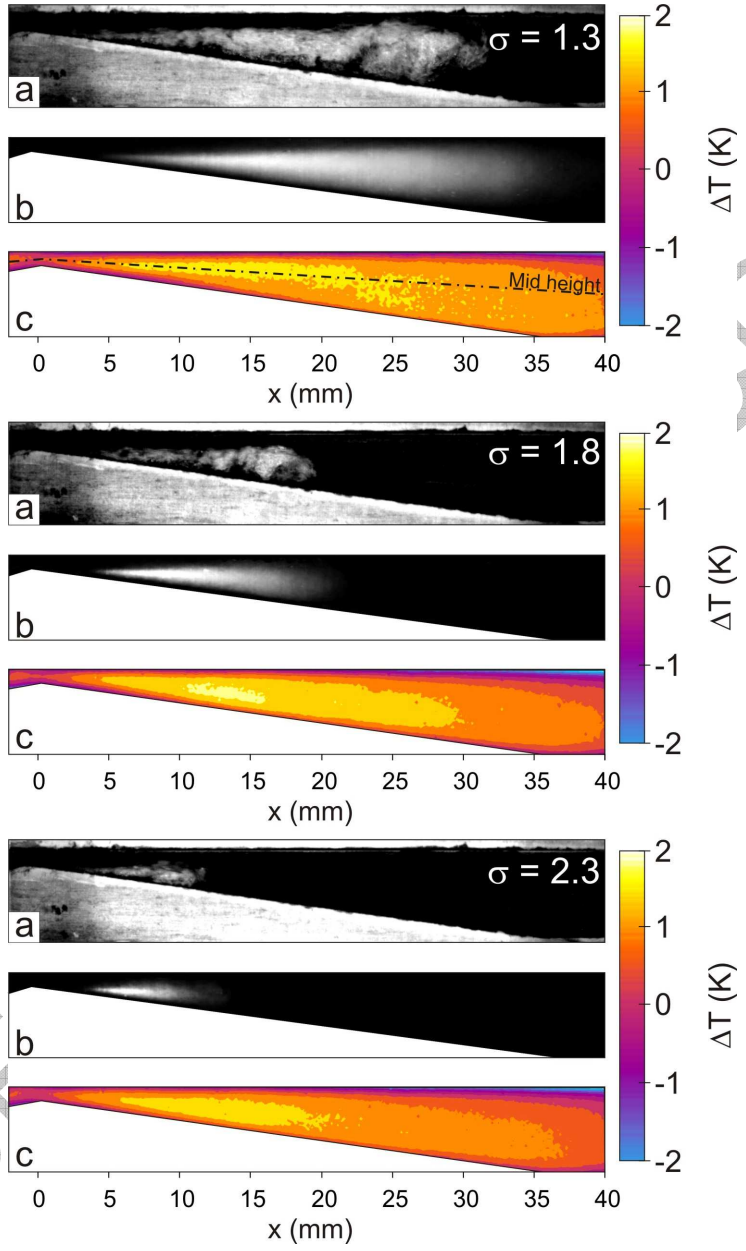


**Figure 4.** Representative instantaneous image of cavitation (a), mean of a series of cavitation images (b) and the mean temperature field (c) for σ = 1.3 (top), σ = 1.8 (middle) and σ = 2.3 (bottom).

The cavitation numbers were chosen on the base of cavity length – for the case of σ = 1.3 the cavitation extends almost over the whole channel – its maximal length was about to 35 mm. The maximal length of cavitation structure at σ = 1.8 was 20 mm what corresponds to roughly a half of the length of the diverging part of the

Venturi channel. The cavitation at $\sigma$ =2.3 occupied one fourth of the channel length – about 10 mm.

As a consequence of cavitation bubble growth by evaporation and gas expansion in the vicinity of the throat a clear temperature depression can be observed. The bubbles then start to collapse what causes rapid recuperation of the temperature which finally exceeds the initial (freestream) temperature. After the peak temperature is achieved, it slowly falls and limits to the freestream temperature at the downstream end of the observation window.

Similarly to the findings of Franc *et al.* (2010) the results imply, to some extent, that the magnitude of the temperature depression is associated to the cavitation number (the cavitation extent) – the larger the cavitation number the smaller the depression. At the present time we feel that more measurements are needed for a clear conformation. Also the temperature fields (images c) closely resemble the mean of a series of cavitation images (images b) – when cavitation extent is greater a larger volume of the fluid is at an elevated temperature and the fall to the freestream temperature occurs further downstream.

It is common for all three cases that cavitation structures cannot be seen just downstream of the throat. The reason for this could be that a large bubble (a few mm in length) first forms in this region, from which smaller bubbles shed – the light scattering on smaller bubbles is more intense, hence they appear whiter in the image. Also one can observe the sheet cavitation in this region must be very thin (less than 1 mm) what implies that it was poorly illuminated during the experiment.

All three cases also share the fact that the bulk fluid is hotter than the one near the bottom and top channel walls. This could be related to the heat flow due to the different temperatures of the fluid and the channel walls. Prior to the experiment the system (test section) was stabilized at a temperature close to the temperature of the water (95°C) by running non cavitating flow through it for a couple of minutes. Since the flow is highly turbulent also the thermal boundary layer should be very small but it seems that we were unable to entirely prevent the heat transfer between the walls and the fluid.

For a more detailed discussion and possible comparisons with simulations it is more convenient to plot diagrams of the temperature evolution along the mid height of the Venturi channel (see Fig. 4) – these are shown in Fig. 5 ($\sigma$ = 1.3 (top), 1.8 (middle) and 2.3 (bottom)).

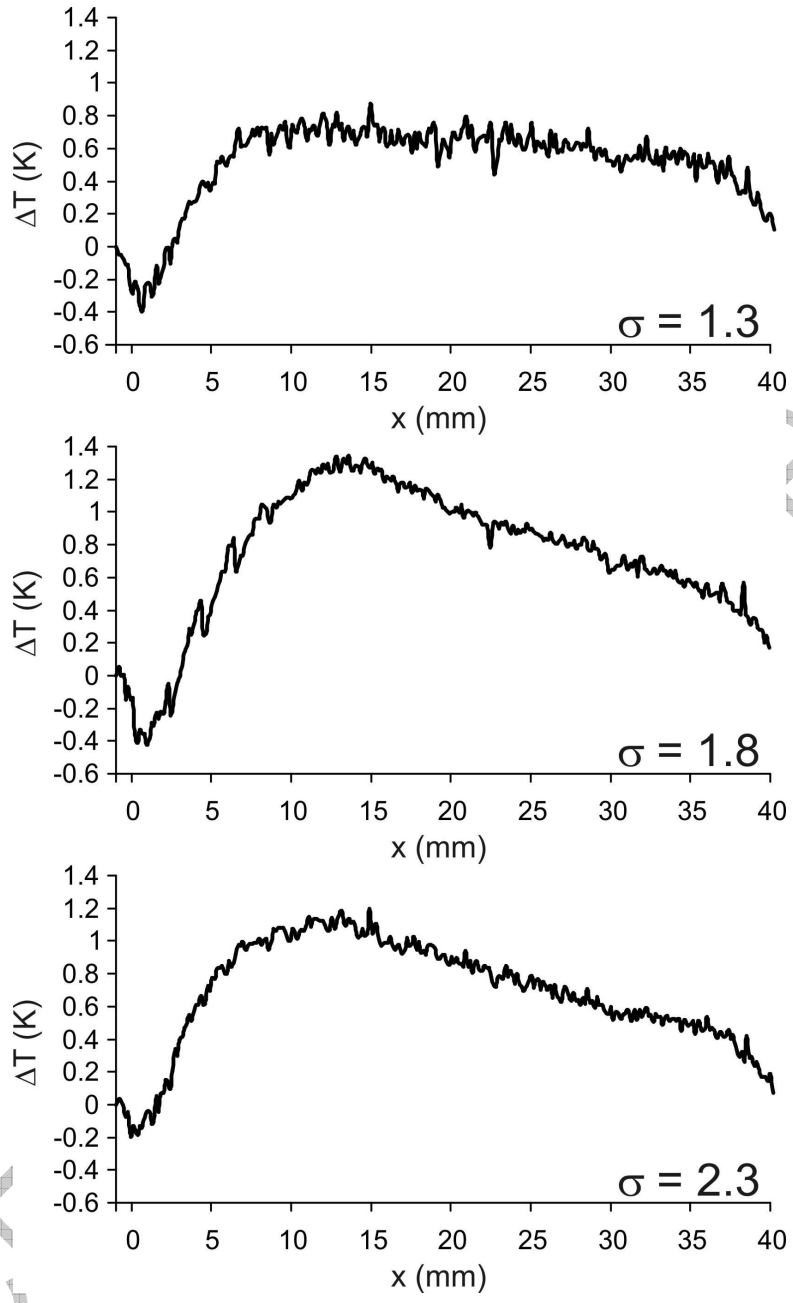


**Figure 5.** Temperature evolution along the mid height of the Venturi channel at σ = 1.3 (top), σ = 1.8 (middle) and σ = 2.3 (bottom)..

As already mentioned the magnitude of the temperature depression is rather unclearly related to the cavitation number (Fig. 5) – according to Franc *et al.* (2004, 2010), it should decrease with the rise of cavitation number. One can see that its value is about ΔT = - 0.2 K for σ = 2.3 and about ΔT = - 0.4 K for both σ = 1.8 and σ = 1.3. If the magnitude of the temperature is in fact unrelated to the cavitation number the reason for this could lie in the rate of growth of cavitation bubbles downstream of the throat of the Venturi section. It is possible that the

rate of bubble growth, which is a dominant parameter in the magnitude of the temperature depression (Eqn. 3), is similar for smaller cavitation numbers and somewhat smaller for the case at $\sigma$ = 2.3. This hypothesis however cannot neither be confirmed nor rejected at the present time.

Interestingly the gradient of the position at which the minimum temperature is measured is similar for all cases (1 mm downstream of the throat; x ≈ 1 mm). This points to a very small region where initial (the first) evaporation takes place.

The temperature then rapidly increases and exceeds the freestream temperature. In cases of lower cavitation numbers a clear temperature peak is achieved approximately at a position of the cavitation cloud separation (at x ≈ 14 mm and x ≈ 10 mm for $\sigma$ = 1.8 and $\sigma$ = 2.3, respectively). This (attached cavity closure) region is many times associated with high pressure oscillations (Wang et al. 2012), which could cause condensation and consequently significantly contribute to the increase of the temperature in this region. In the case at $\sigma$ = 1.3 we did not measure the temperature peak. The almost constant (only gradually decreasing) temperature profile can be associated to a much larger cavitation extent, which at some instants limits to supercavitating conditions.

If one assumes the cavitation bubble to grow and collapse only one time (according to the theory – Eqn. 3), the temperature evolution should be quite different – one should see a rapid decrease of the temperature which would be followed by an even greater but shorter temperature increase, afterwards the temperature should again rapidly fall to the freestream temperature. Measurements agree with the single bubble approach theory for the part of the temperature depression (bubble growth). The trend downstream can be explained if one accepts the fact that the bubbles rebound several times as they flow through the Venturi section. At $\sigma$ = 1.3 the low pressure region is larger what causes more bubble rebounds and leads to a more constant temperature profile then in cases at higher cavitation numbers. In Section 5 a prediction of the thermodynamic effects, where bubble rebounds were considered, is shown.

**4.2 Temperature field dynamics**

In the second set of measurements we investigated the dynamics of the temperature field. For this we needed to increase the acquisition frequency of the IR camera to about 3550 Hz. Consequently we had to decrease size of the observation window, which now extended only 15 mm downstream of the throat. Figure 6 shows the instantaneous images captured with the high-speed (left) and IR (right) cameras.

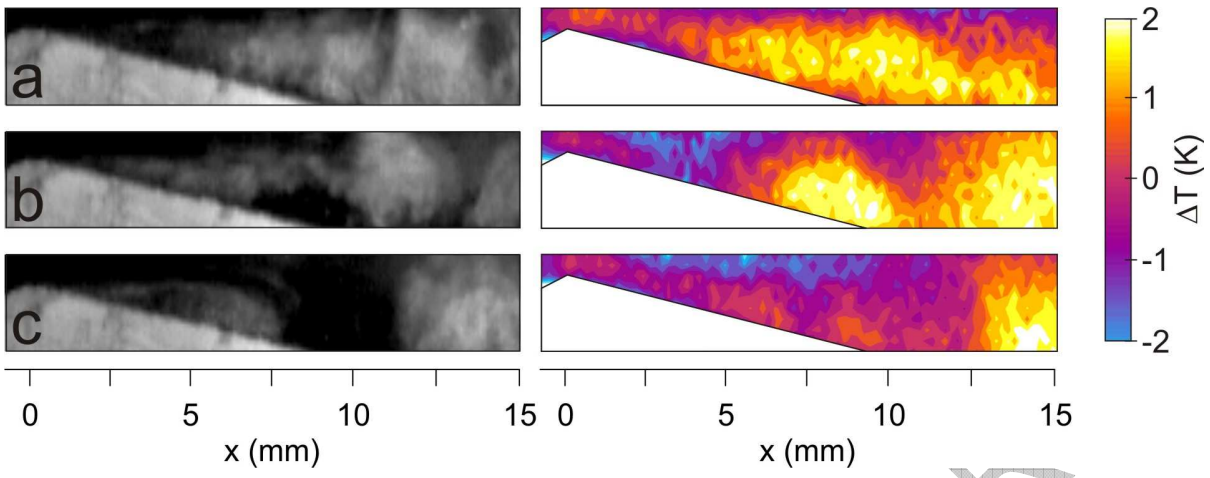


**Figure 6.** Instantaneous images of cavitation and the corresponding temperature field at σ = 1.8.

As already mentioned cavitation near the throat of the Venturi cannot be clearly seen. One can see that cavitation clouds, which consist of a large number of tiny bubbles, posses a higher temperature than the rest of the flow. This again confirms the hypothesis the bubbles inside the cloud undergo several rebounds in their lifetime. If a bubble would undergo only one growth and collapse, the cloud should either be cold (if the bubble would still be growing) or of the same temperature as the rest of the fluid (if the bubble would be at a quasi stable state before its collapse), the "hot" region would then appear only for a short period of time, just after the cloud collapse. The synchronicity jitter between the two cameras (case b), comes from the inability of setting exact frame rate of the IR camera. It could be set within 0.15% of the desired value and exactly determined a posteriori - this caused the capture of the images to deviate as the time progressed.

For a clearer comparison of the temperature and cavitation dynamics and to avoid the influence of the synchronicity jitter one dimension of the recorded data was sacrificed – the temperature differences ΔT and the intensity of cavitation structures ϕ at the mid height of the channel (see Fig. 4) were first taken from each image and were then stacked together in a time diagram in Fig. 7. The intensity of cavitation structures ϕ is calculated as the brightness of the structure in the image (in % – white ϕ = 100%, black ϕ = 0%) and could roughly be related to the void fraction. The time is reported on the y axis, while the x axis represents the distance from the Venturi throat. Cavitation intensity is shown in the left and the temperatures in the right diagram. Results for all cavitation numbers are shown (σ = 1.3 (top), 1.8 (middle) and 2.3 (bottom)).

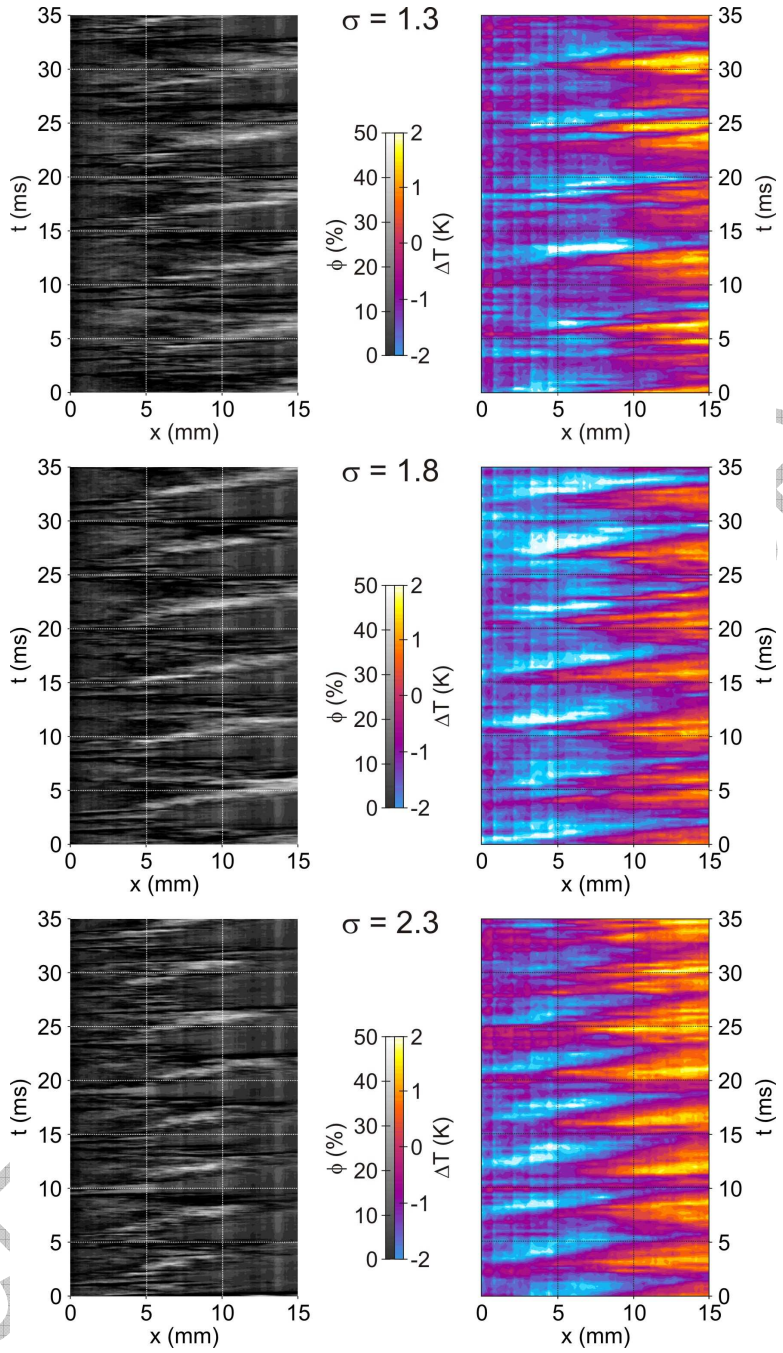


**Figure 7.** Intensity of cavitation structures ϕ and the temperature differences ΔT as a function of space (distance from the Venturi throat) and time for σ = 1.3 (top), 1.8 (middle) and 2.3 (bottom).

We see that both the cavitation structures and the temperatures exhibit vivid dynamics. By moving along the y (time) axis one can see that maximum of cavitation intensity moves from the throat further downstream, what points to the shedding of cavitation clouds. The region of higher temperature at first follows the movement of the cavitation cloud, but later on (near the position of cloud collapse) somewhat diffuses – this is particularly well

seen for the case of $\sigma = 2.3$ where at the end of the observation window the temperature is almost constant in time. We believe that this is a result of heat convection after the cloud collapse. In the case of $\sigma = 1.3$ and 1.8 this phenomenon cannot be seen since the clouds imploded further downstream (the observation window extended only 15 mm downstream of the throat). The position of the observation window also prevented us to observe temperature decrease to the freestream level what was nicely seen in mean temperature profiles (Figs. 4 and 5).

The shedding and the temperature dynamics are obviously periodic and closely related. The eigenfrequencies of the phenomenon lie at 166, 200 and 225 Hz for $\sigma = 1.3$, 1.8 and 2.3, respectively. One can see that the cavitation structures near the throat of the Venturi are cold and they heat up as they flow downstream. In short intervals, when there is almost no cavitation present, the temperature profile seems to be almost constant (for example for $\sigma = 1.8$ at t = 18 ms).

**5 Comparisons to the theory of thermal delay**

One of the goals of the study was to investigate whether the thermal delay theory (presented in section 3) can be applied to the cavitating flow problems. The thermal delay theory was developed only for a case of a single cavitation bubble and more complex approaches are scarce – mainly due to the lack of experimental data. In the present work we limited our investigation to the question if experimental results roughly comply with the theory. As a test condition we took the case at $\sigma = 1.3$.

First we calculated the pressure evolution along the mid height (see Fig.4) of the Venturi channel. One could do this by CFD, but to limit the number of adjustable variables and consequently to leave the investigation as clear and as simple as possible this was done by a potential flow theory approach (Gaston *et al.* 2001). Here one calculates that as the flow approaches the throat of the Venturi the pressure rapidly drops from $p_1$ to vapour pressure, which persists about 6 mm downstream of the throat. During the next 12 mm the pressure then recovers to approximately pressure $p_2$. The pressure losses were also considered.

Since we are dealing with cavitating flow, one should consider the possibility of interaction between the bubbles. This was intentionally omitted, again for the sake of clarity of results. We do not know the size of the cavitation nuclei as they enter the Venturi channel. Hence an ensemble of nuclei sizes was chosen ($R_0$ = 1, 1.5, 2, 2.5 and 3 μm), which, according to the modified Rayleigh-Plesset equation (Eqn. 5), grew to a maximal bubble radius recorded during the experiment – this was estimated from the images and was in the order of 5 to 10 μm.

Figure 8 shows the calculated temperature evolutions (according to Eqn. 3) for 5 cavitation nuclei sizes together with experimental results for the case of $\sigma = 1.3$.

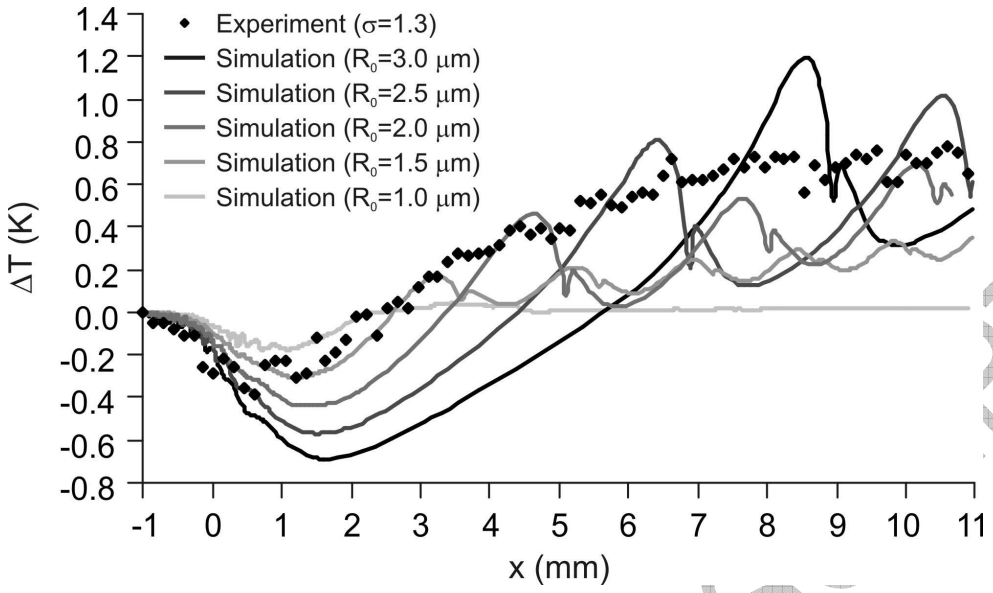


**Figure 8.** Calculated and measured temperature evolutions in the mid height of the channel for the case of σ = 1.3.

One can see that the size of the nuclei plays a major role in the temperature evolution. An approach where an ensemble of nuclei sizes was used to calculate the temperature profile is just, since the nuclei do not have an exact size. One can see that the bubbles undergo one or more rebounds as they flow through the low pressure zone. As already mentioned a single growth and collapse would result in a rapid cooling and heating of the fluid. On the other hand a number rebounds reveals a temperature profile which first drops below the freestream temperature and then gradually rises to a higher temperature – a trend which was observed during experiments.

## 7 Conclusions

There is a great need for experimental data for evaluation and further development of methods for the prediction of thermodynamic effects of cavitation. Due to the complexity of the measurements the existing experimental data is extremely scarce – the most advanced numerical techniques base on evaluation against the measurements made in the 1960's and 1970's.

In the present work we show high speed IR camera measurements of the temperature fields in cavitating flow of hot water, which already exhibits measurable (if not significant) thermal delay. For the first time the temperature fields across the Venturi section were obtained and the temperature dynamics was observed.

Results show that the idea of the thermal delay can be applied to the present problem, but one needs to consider the possibility (probability) that a bubble rebound occurs.

Further work will include measurements in a larger Venturi section, observations from the bottom side of Venturi and other fluids than water.

**Acknowledgment**

The authors would like to thank the European Space Agency (ESA), for the financial support in the scope of the project “Cavitation in Thermosensible Fluids”.

**References**

Brennen, C. E. 1973 The Dynamic Behavior and Compliance of a Stream of Cavitating bubbles. ASME *J. Fluids Eng.*, **95** (4), 533-541.

Brennen, C.E 1995 Cavitation and Bubble Dynamics, Oxford University Press.

Cervone, A., Testa, R. & d'Agostino, L. 2005 Thermal Effects on Cavitation Instabilities in Helical Inducers. *J. Propul. Power*, **21**, 893–899.

Dular, M., Bachert, R. 2009 The issue of Strouhal number definition in cavitating flow. *J. mech. eng.*, **55**, 11, 666-674.

Dular, M., Khlifa, I., Fuzier, S., Adama Maiga, M., Coutier-Delgosha, O. 2010 Scale effect on unsteady cloud cavitation. *Exp. fluids*, **53** (5), 1233-1250

Dular, M., Coutier-Delgosha, O. 2012 Thermodynamic effect at a single cavitation bubble growth and collapse. Proceedings of the 8th International Symposium on Cavitation CAV2012 – Submission No. 53, August 14-16, 2012, Singapore.

Franc, J.-P. & Michel, J.-M 2004 Fundamentals of Cavitation. Fluid Mechanics and Its Applications, **76**, Springer.

Franc, J.-P., Rebattet, C., & Coukon, A. 2004 An Experimental Investigation of Thermal Effects in a Cavitating Inducer,” *ASME J. Fluids Eng.*, **126**, 716–723.

Franc, J.-P., Boitel, G., Riondet, M., Janson, E., Ramina, P. & Rebattet, C. 2010 Thermodynamic Effect on a Cavitating Inducer-Part II: On-Board Measurements of Temperature Depression Within Leading Edge Cavities. ASME *J. Fluids Eng.*, **132** (2), 021304.

Fruman, D.H., Reboud, J.L. & Stutz, B. 1999 Estimation of thermal effects in cavitation of thermosensible liquids. *Int. Journal of Heat and Mass Transfer*, **42**, 3195-3204.

Gaston, M.J., Reizes, J.A., Evans, G.M. 2001 Modelling of Bubble Dynamics in a Venturi Flow with a Potential Flow Method, Chemical Engineering Science, **56,** 6427-6435.

Goncalvès, E., Fortes Patella R. 2010 Numerical study of cavitating flows with thermodynamic effect, Computers & Fluids, **39**, 99–113.

Goncalvès, E., Fortes Patella R. 2011 Constraints on equation of state for cavitating flows with thermodynamic effects, Applied Mathematics and Computation, **217**, 5095–5102.

Goncalvès, E., Fortes Patella R., Rolland J., Pouffary B., Challier G. 2010 Thermodynamic Effect on a Cavitating Inducer in Liquid Hydrogen, Journal of Fluids Engineering, **132**, 111305-1.

Hale G. M. & Querry M. R. 1973 Optical constants of water in the 200 nm to 200 μm wavelength region. *Appl. Opt.*. **12**, 555-563.

Hauke, G. , Fuster, D. & Dopazo, C. 2007 Dynamics of a single cavitating and reacting bubble. *Physical Review E*, **75**, 066310.

Hord, J., Anderson L. M., Hall W. J. 1972 Cavitation in Liquid Cryogens I – Venturi. *NASA CR-2054.*

Hord, J. 1973a Cavitation in Liquid Cryogens II – Hydrofoil. *NASA CR-2156.*

Hord, J. 1973b Cavitation in Liquid Cryogens III – Ogives. *NASA CR-2242.*

Hosangadi, A., Ahuja, V. 2005 Numerical study of cavitation in cryogenic fluids, Journal of Fluids Engineering, **127** (2), 267–281.

Kato, H. 1984, Thermodynamic Effect on Incipient and Development of Sheet Cavitation. *Proceedings of International Symposium on Cavitation Inception*, New Orleans, LA, 127-136.

Plesset, M. S. 1949 The dynamics of cavitation bubbles. *J. Appl. Mech.*, **16**, 277-282.

Rimbert, N., Castanet, G., Funfschilling, D. 2012 Experimental Study by Two-Colors Laser-Induced-Fluorescence of the Thermodynamic Effect in Micro-Channel Cavitation. Proceedings of the 8th International

Symposium on Cavitation CAV2012, August 14-16, 2012, Singapore.

Ruggeri, R.S., & Moore, R.D. 1969 Method for Prediction of Pump Cavitation Performance for Various Liquids, Liquid Temperature, and Rotation Speeds. *NASA TN, D-5292.*

Sarosdy L. R & Acosta A. J. 1961 Note on observations of cavitation in different fluids. *ASME J. Basic Eng.*, **83**, 399-400.

Sekita, R., Watanabel, A., Hirata, K. & Imoto, T. 2001 Iessons learned from H-2 failure and enhancement of H-2a project. *Acta Astronautica,* **48** (5-12), 431-438.

Stahl, H. A. & Stepanoff, A. J. 1956 Thermodynamic Aspects of Cavitation in Centrifugal Pumps. *ASME J. Basic Eng.*, **78**, 1691-1693.

Stepanoff A. J. 1961 Cavitation in centrifugal pumps with liquids other than water. *J. Eng. Power*, **83**, 79-90

Utturkar, Y., Wu, J., Wang, G., Shyy, W. 2005 Recent progress in modelling of cryogenic cavitation for liquid rocket propulsion, Progress in Aerospace Sciences, **41**, 558–608.

Wang, Y., Yuan, X., Zhang, Y. 2012 Experimental investigation on the pressure characteristics of cavity closure region. Journal of Marine Science and Application, **11** (4), 462-468.

Watanabe, S., Hidaka, T., Horiguchi, H., Furukawa, A. & Tsujimoto, Y. 2007 Steady Analysis of the Thermodynamic Effect of Partial Cavitation Using the Singularity Method. *ASME J. Fluids Eng.*, **129** (2), 121-127.